Quasimonoenergetic electrons from unphased injection into channel guided laser wakefield accelerators

D. F. Gordon,[1] R. F. Hubbard,[1] J. H. Cooley,[1,2,3] B. Hafizi,[2] A. Ting,[1] and P. Sprangle[1]
[1]*Naval Research Laboratory, Plasma Physics Division, Washington, D.C. 20375, USA*
[2]*Icarus Research, Inc., P.O. Box 30780, Bethesda, Maryland 20824-0780, USA*
[3]*University of Maryland, College Park, Maryland 20742, USA*
(Received 27 July 2004; revised manuscript received 11 November 2004; published 11 February 2005)

A high-quality electron beam can be extracted from a channel guided laser wakefield accelerator without confining the injected particles to a small region of phase. By careful choice of the injection energy, a regime can be found where uniformly phased particles are quickly bunched by the accelerator itself and subsequently accelerated to high energy. The process is particularly effective in a plasma channel because of a favorable phase shift that occurs in the focusing fields. Furthermore, particle-in-cell simulations show that the self-fields of the injected bunches actually tend to reduce the energy spread on the final beam. The final beam characteristics can be calculated using a computationally inexpensive Hamiltonian formulation when beam-loading effects are minimal.

DOI: 10.1103/PhysRevE.71.026404 PACS number(s): 52.38.Kd, 41.75.Jv, 41.75.Ht, 52.65.Rr

I. INTRODUCTION

The laser wakefield accelerator (LWFA) is potentially a compact and inexpensive source of high-energy electrons [1–3]. It utilizes a short pulse laser to drive a plasma wave which can be used as an ultrahigh gradient accelerating structure. In a uniform plasma, the length of the accelerator is limited to the Rayleigh length associated with the minimum spot size of the laser pulse. This limitation can be removed by guiding the laser pulse in a plasma channel or other structure [4–9]. Using currently available chirped-pulse amplification lasers [10,11] such a system could generate GeV electrons in a length on the order of 10 cm [12–15].

In a LWFA the accelerated electrons can be taken from the background plasma as well as from externally injected particles. In the long-pulse "self-modulated" regime ($\tau_L \gg 2\pi/\omega_p$, where τ_L is the laser pulse length and ω_p is the plasma frequency) the acceleration of particles from the background plasma tends to produce a beam with 100% energy spread [16–19]. More recently, quasimonoenergetic acceleration of particles from the background plasma has been observed in simulations [20,21] and experiments [22–24] operating in a shorter-pulse regime. Thus far, these experiments have suffered from poor shot-to-shot stability. Simulations suggest that stable production of monoenergetic electron beams can be achieved by operating in the resonant LWFA regime ($\tau_L \sim \pi/\omega_p$) with a moderate intensity driver ($a \lesssim 1$, where a is the normalized vector potential) and by injecting electrons from an external source [25]. It has generally been believed that the injected electrons must be phased to within a small fraction of a plasma period in order to produce a high-quality beam, although some counterexamples have been offered [26–28]. For typical LWFA parameters this would require that the injected electrons and the driving laser pulse be synchronized to within tens of femtoseconds and that the length of the injected electron pulse be similarly short. A variety of optical injection schemes have been proposed to meet this requirement [29–33].

This paper presents a study of the particle orbits in a typical channel-guided LWFA which demonstrates that such tight bunching of the injected electrons is not always necessary. If the injected electrons are initially monoenergetic, the accelerating structure itself possesses a phase bunching property which can be exploited by carefully choosing the injection energy. Even when all the phases are uniformly loaded, a substantial fraction of the particles can be bunched and monoenergetically accelerated within the same device. The remainder of the particles are either radially expelled or left behind as a much lower-energy beam. By tuning the injection energy to the amplitude of the wakefield, a trade-off can be made between the charge in the accelerated beam and the energy spread. This process involves removal or pruning of electrons that fall into the defocusing portion of the wake, combined with strong phase bunching and rapid acceleration. Interestingly, the process becomes even more effective when there is substantial beam loading. The possibility of using a long, "unphased" injected electron pulse raises the possibility of using more conventional injector technology in place of all-optical injection.

The outline of the remainder of this paper is as follows. Section II describes a quasi-two-dimensional (quasi-2D) Hamiltonian model that describes the dynamics of monoenergetic electrons loaded uniformly over all phases of a LWFA. Section III applies this model to the calculation of trapping efficiencies and energy spreads for typical LWFA parameters. Section IV presents turboWAVE [34] simulations of the process and compares the results to the Hamiltonian model. Section V summarizes the work and discusses implications for future LWFA experiments.

II. HAMILTONIAN FORMULATION

A. Basic formulation and phase space orbits

The orbits of test electrons in a one-dimensional LWFA are often studied by plotting contours of the Hamiltonian,

which in the wave frame is a constant of the motion. The Hamiltonian in the wave frame expressed in laboratory frame coordinates is [3]

$$H(\gamma,\psi) = \gamma(1-\beta_g\beta)mc^2 + q\phi_0 \sin\psi, \tag{1}$$

where β is the velocity of the particle normalized to the speed of light c, $\gamma=(1-\beta^2)^{-1/2}$, $v_g=c\beta_g$ is both the group velocity of the laser pulse and the phase velocity of the plasma wave, m is the mass of the particle, q is the charge of the particle, and the accelerating field is described by the electrostatic potential $\phi=\phi_0 \sin\psi$. Here, $\psi=\omega_p(z/v_g-t)$, where ω_p is the plasma frequency, z is the longitudinal coordinate of the particle, and t is time. The Hamiltonian in Eq. (1) is valid for test particles in one dimension and assumes that the plasma wave has a low enough amplitude so that harmonics can be neglected. Although the Hamiltonian is one dimensional, transverse effects can be partly accounted for by assuming that particles crossing into defocusing regions are lost due to radial expulsion. In a uniform plasma, the focusing region is defined by $2\pi n<\psi<2\pi(n+1/2)$, where n is an integer. In a plasma channel the focusing region is larger [35], which can significantly improve the performance of the accelerator, as will be seen below.

The contours of $H(\gamma,\psi)$ for a wave with amplitude $|e|\phi/mc^2=10^{-4}$ are shown in Fig. 1(a), and those for a wave with amplitude $|e|\phi/mc^2=0.1$ are shown in Fig. 1(b). In both cases, $\gamma_g=1/\sqrt{1-\beta_g^2}=59$ which corresponds to a plasma density of 5×10^{17} cm^{-3} assuming an 800-nm laser pulse is the driver. A particle introduced into either wave is constrained to move along a single contour. If $\gamma>\gamma_g$, the particles move from left to right. If $\gamma<\gamma_g$, the particles move from right to left. The closed orbits correspond to trapped particles and the open orbits to untrapped particles. The stationary point lies at $\gamma=\gamma_g$ and $\psi=\pi/2$. In the small-amplitude case, the closed orbits are symmetric about the line $\gamma=\gamma_g$. In the large-amplitude case, this symmetry is broken by relativistic effects. In particular, the particle must spend more time overtaking the wave than falling behind it due to the fact that the velocity changes very little at high energies.

In a plasma channel, the boundaries of the focusing region depend on the channel parameters. We therefore consider the general case where the focusing region is defined by $\psi_-<\psi<\psi_+$. The largest closed orbit that satisfies $\psi>\psi_-$ contains all the orbits corresponding to particles that never cross into the defocusing region as they are accelerated. This "retaining orbit" is defined by $H(\gamma,\psi)=H(\gamma_g,\psi_-)$. The contour tangent to the dashed line in Fig. 1(a) is an example where $\psi_-=0$ (uniform plasma). The highest point on the retaining orbit gives the largest energy a particle can obtain assuming that $\gamma_0<\gamma_g$ where γ_0 is the injection energy. The lowest point on the retaining orbit gives the minimum injection energy. These two energies can be determined by solving $H(\gamma,\psi)=H(\gamma_g,\psi_-)$ for γ and evaluating the solution at $\psi=\pi/2$. Defining $\bar{\phi}=q\phi_0(\sin\psi_- -1)/mc^2$, the result is

$$\gamma_\pm = \gamma_g + \gamma_g^2\bar{\phi} \pm \sqrt{(\bar{\phi}^2\gamma_g + 2\bar{\phi})(\gamma_g^3-\gamma_g)}. \tag{2}$$

Injection of a monoenergetic beam into the wave can be visualized as follows. Imagine a horizontal line superimposed on the contours at a vertical position between γ_- and γ_+. Each point on the line represents the initial phase space coordinate of an injected particle. The phase space trajectory corresponding to each initial condition is simply the contour intersecting the line at that point. The dashed line in Fig. 1(a) corresponds to a scenario where the injection energy is γ_-. In this case, all particles are lost except those at $\psi=\pi/2$. Although the final energy spread would vanish, so would the charge. By increasing the injection energy, the charge collected increases but so does the energy spread. The problem is to quantify the proportion in which these two quantities increase as the injection energy is raised.

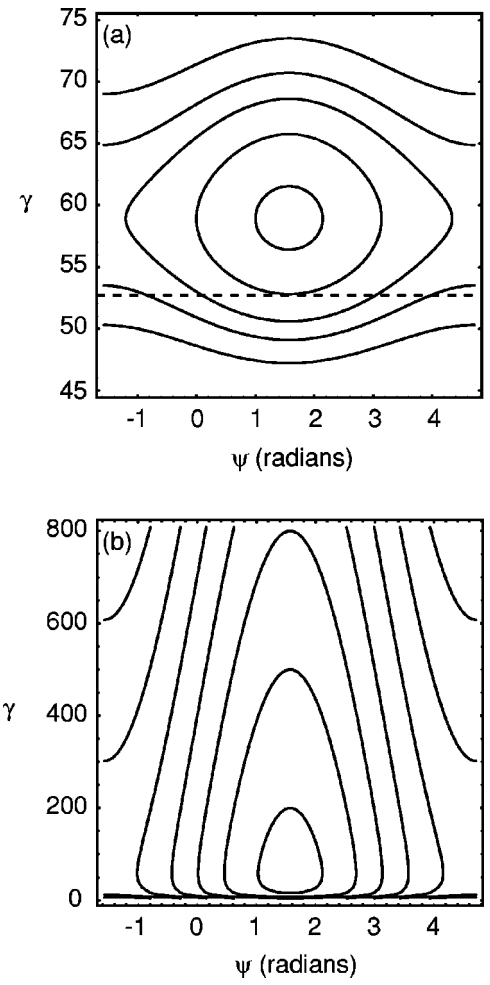

FIG. 1. Contours of the Hamiltonian. (a) Particle orbits for a wave with $e\phi_0/mc^2=10^{-4}$. (b) Particle orbits for a wave with $e\phi_0/mc^2=0.1$. The dashed line in (a) is tangent to the retaining orbit and indicates the minimum injection energy.

B. Collection efficiency and dephasing length

The collection efficiency is defined as the ratio of the charge emerging from the end of the accelerator to the charge injected. For monochromatic injection, the collection efficiency is

$$\eta = \frac{\psi_{max} - \psi_{min}}{2\pi}, \tag{3}$$

where $\psi_{min} < \psi < \psi_{max}$ defines the set of initial phases for which particles with initial energy γ_0 never cross into defocusing regions of the wave. Graphically, this interval corresponds to the segment of the line $\gamma = \gamma_0$ contained within the retaining orbit. The end points of the line segment can be found by solving $H(\gamma_0, \psi_{min}) = H(\gamma_g, \psi_-)$ for ψ_{min} with the result that

$$\psi_{min} = \sin^{-1}\left[\frac{\gamma_g^{-1} - \gamma_0(1 - \beta_g\beta_0) + q\phi_0 \sin \psi_-/mc^2}{q\phi_0/mc^2} \right], \tag{4}$$

where we choose the solution satisfying $\psi_- < \psi_{min} < \pi/2$. In a uniform plasma ψ_{max} can be found using the fact that the focusing fields are symmetric about $\psi = \pi/2$. In a plasma channel, however, the focusing fields are shifted toward negative ψ which introduces an additional constraint:

$$\psi_{max} = \min\{\pi - \psi_{min}, \psi_+\}. \tag{5}$$

The final energy spread can only be computed once the length of the accelerator is specified. The distance traveled by any particle is the time-integrated velocity $z = \int \beta c dt$. The velocity can be expressed in terms of the phase by solving $H(\gamma, \psi) = H_0$ for β where $H_0 = H(\gamma_0, \psi_0)$, and (γ_0, ψ_0) is the initial phase space coordinate of the particle. The result is

$$\beta_\pm(\psi) = \frac{\beta_g \pm \sqrt{f^2(f^2 + \beta_g^2 - 1)}}{\beta_g^2 + f^2}, \tag{6}$$

where $f = (H_0 - q\phi_0 \sin \psi)/mc^2$. With a change of variables, the integral over time can be converted to an integral over phase, giving

$$z = \int_{\psi_1}^{\psi_2} \nu_\pm d\psi, \tag{7}$$

where

$$\nu_\pm = \beta_\pm c \left[\omega_p \left(\frac{\beta_\pm}{\beta_g} - 1 \right) \right]^{-1}. \tag{8}$$

If $\beta > \beta_g$, one uses ν_+ and $\psi_2 > \psi_1$ when evaluating the integral. If $\beta < \beta_g$, one uses ν_- and $\psi_2 < \psi_1$ when evaluating the integral.

To construct the integral representing the length of the accelerator, the phases at which the particle velocity is β_g must be known. These can be found by solving $H(\gamma_g, \psi_g) = H_0$ for ψ_g. The solutions are given by

$$\psi_g = \sin^{-1}\left(\frac{H_0}{q\phi_0} - \frac{mc^2}{\gamma_g q\phi_0} \right). \tag{9}$$

The dephasing length L_d can be defined as the distance for which electrons injected at $\psi = \psi_{min}$ reach the phase $\pi/2$. The solution to Eq. (9) in the quadrant $0 < \psi_g < \pi/2$ corresponds to the point at which these particles begin to move forward in phase. For $z > L_d$, these particles are decelerated, so L_d represesents the maximum useful length for single stage acceleration. Using this solution along with Eqs. (6)–(8), the dephasing length is given by

$$L_d = \int_{\psi_{min}}^{\psi_g} \nu_- d\psi + \int_{\psi_g}^{\pi/2} \nu_+ d\psi. \tag{10}$$

It should be noted that in the evaluation of L_d a singularity occurs in the integrand at ψ_g. However, the singularity is integrable and can be evaluated without difficulty using off-the-shelf mathematical software. In our work we used the software package Mathematica.

C. Final beam energy and phase characteristics

With the length of the accelerator known, the output energy and phase of each particle can be computed. By making a change of variables on the momentum equation $dp/dt = -q\nabla\phi$ and the equation of phase evolution $d\psi/dt = (v - v_g)\omega_p/v_g$, and using $\nabla\phi = \phi_0(\omega_p/v_g)\cos\psi$, two coupled ordinary differential equations are obtained for the momentum and phase as a function of distance propagated [36]:

$$\frac{dp}{dz} = -q\phi_0 \frac{\omega_p}{v_g} \left(\frac{m^2}{p^2} + \frac{1}{c^2} \right)^{1/2} \cos \psi, \tag{11}$$

$$\frac{d\psi}{dz} = \omega_p \left[\frac{1}{v_g} - \left(\frac{m^2}{p^2} + \frac{1}{c^2} \right)^{1/2} \right]. \tag{12}$$

Again, these equations can be integrated from $z = 0$ to $z = L$ using standard off-the-shelf software. The result is the output energy and phase as a function of the input energy and phase. Let the output energy be denoted $\gamma_f(\gamma_0, \psi_0)$ and the output phase be denoted $\psi_f(\gamma_0, \psi_0)$. Then for monochromatic injection at $\gamma = \gamma_0$ the mean output energy $\langle\gamma\rangle$ and root-mean-squared (rms) energy spread $\delta\gamma$ are given by

$$\langle\gamma\rangle = \frac{1}{2\pi\eta} \int_{\psi_{min}}^{\psi_{max}} \gamma_f(\gamma_0, \psi_0) d\psi_0, \tag{13}$$

$$\delta\gamma^2 = \frac{1}{2\pi\eta} \int_{\psi_{min}}^{\psi_{max}} [\gamma_f(\gamma_0, \psi_0) - \langle\gamma\rangle]^2 d\psi_0, \tag{14}$$

while mean output phase $\langle\psi\rangle$ and rms pulse width $\delta\psi$ are given by

$$\langle\psi\rangle = \frac{1}{2\pi\eta} \int_{\psi_{min}}^{\psi_{max}} \psi_f(\gamma_0, \psi_0) d\psi_0, \tag{15}$$

$$\delta\psi^2 = \frac{1}{2\pi\eta} \int_{\psi_{min}}^{\psi_{max}} [\psi_f(\gamma_0, \psi_0) - \langle\psi\rangle]^2 d\psi_0. \tag{16}$$

Equations (13)–(16) quantify the beam quality of a LWFA when the injected particles are loaded into all phases but at a single energy.

III. HAMILTONIAN ANALYSIS OF UNPHASED, MONOENERGETIC INJECTION

Using the formulas from Sec. II we wrote a Mathematica program to calculate $\delta\gamma$ and $\delta\psi$ given an injection energy γ_0,

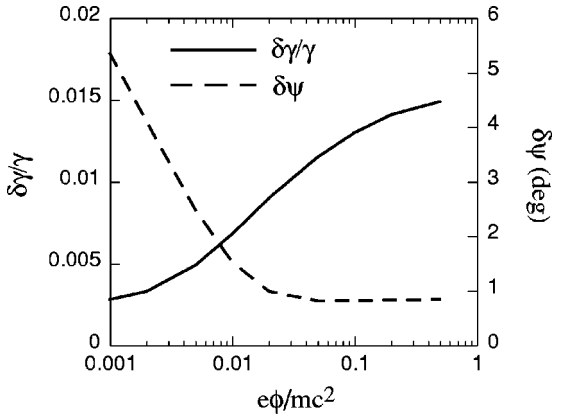

FIG. 2. Relative energy spread $\delta\gamma/\gamma$ and phase spread $\delta\psi$ vs wave amplitude holding the collection efficiency fixed at 10% and evaluating at the end of the accelerator.

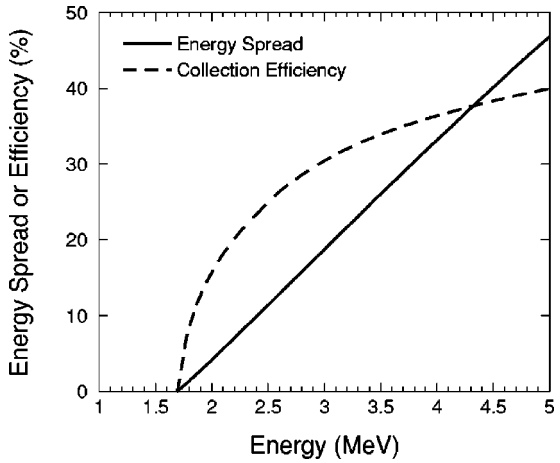

FIG. 3. Collection efficiency η and energy spread $\delta\gamma/\gamma$ vs injection energy holding wave amplitude fixed at $e\phi_0/mc^2=0.1$. The length of the accelerator was 8.9 cm and the mean output energy was 365 MeV.

a wave amplitude ϕ_0, and a plasma density n_e. In this section, the phasing of the focusing fields was taken to be that of a uniform plasma ($\psi_-=0$, $\psi_+=\pi$). Consider first the effect of wave amplitude. It is not meaningful to hold the injection energy fixed since the range of possible injection energies depends strongly on ϕ_0. Instead, the injection energy for each ϕ_0 may be chosen based on the requirement that a fixed fraction of the injected particles be transported through the entire accelerator. In this case, the injection energy is found from the implicit equation

$$\psi_{min}(\gamma_0,\phi_0,n_e)=\frac{\pi-\eta}{2}, \tag{17}$$

where η is the collection efficiency from Eq. (3). Consider the case where $\eta=0.1$ and $n_e=5\times10^{17}$ cm^{-3}. The energy spread and pulse length as a function of ϕ_0 are plotted in Fig. 2. The results are very favorable. The relative energy spread is on the order of 1% even though 10% of the particles were collected. Furthermore, for a wide range of wave amplitudes the particles are bunched to within 1° of phase when they reach the end of the accelerator. Interestingly, small-amplitude waves give better relative energy spread while large-amplitude waves give better phase bunching.

Next the wave amplitude is held fixed and the injection energy is varied. As discussed below, a wave amplitude of $e\phi_0/mc^2=0.1$ is meaningful in terms of experiments that could be carried out in the immediate future. Using this amplitude along with a density of $n_e=5\times10^{17}$ cm^{-3}, the length of the accelerator is 8.9 cm, the minimum injection energy γ_- is about 1.7 MeV, and the 1D trapping threshold is about 0.7 MeV. The collection efficiency η and the energy spread $\delta\gamma/\gamma$ are plotted as a function of injection energy in Fig. 3. The collection efficiency rises very rapidly as the injection energy is increased and eventually asymptotes to 50% as $\gamma_0\rightarrow\gamma_g$. The energy spread, by contrast, increases linearly over the range of energies plotted. The fact that the collection efficiency rises much faster than the energy spread near γ_- makes unphased monoenergetic injection an attractive possibility.

As a final illustration, Fig. 4 compares the contours of the Hamiltonian for two different injection energies. The wave amplitude and plasma density are again $e\phi_0/mc^2=0.1$ and $n_e=5\times10^{17}$ cm^{-3}. The contours corresponding to injection at 2.14 MeV are shown in Fig. 4(a). The collection efficiency for this case is 20% and the final energy spread is 6.0%. The figure shows that it is primarily the outermost closed orbits that are loaded, and therefore all the particles in the focusing phase of the wave will eventually reach ≈400 MeV. The fact the particles reach ≈400 MeV at the same time can be understood by considering that they spend very little time in the region $\gamma<\gamma_g$ compared with the time they spend in the region $\gamma>\gamma_g$. This is because when $\gamma<\gamma_g$ the energy change caused by the wake has a greater effect on the velocity than when γ is large. The particles therefore get swept back to the point $\psi\approx0$ almost immediately, after which they all move together from $\psi=0$ to $\psi=\pi/2$. In contrast, Fig. 4(b) shows contours corresponding to injection at $\gamma_g\approx30$ MeV. In this case, all the closed orbits are loaded which leads to an energy spread of 100%.

IV. PARTICLE-IN-CELL SIMULATIONS

The conclusions of Sec. III are based on the assumption of exact monochromatic injection of a zero emittance beam into an idealized accelerating structure. It was assumed that the only effect of the transverse fields is to eject particles that stray into the defocusing phases. It was also assumed that the self-fields of the injected bunches are negligible. To test the relevance of the conclusions drawn from this model we turn to the particle-in-cell simulation code turboWAVE [34]. The simulation parameters are chosen to correspond to a channel guided LWFA using a capillary discharge to create the plasma channel and a femtosecond Ti:sapphire laser to drive the plasma wave. The simulations are fully relativistic and fully electromagnetic. They take into account the nonlinear and transverse structure of the plasma wave, the finite emittance and energy spread of the injected electrons, and the

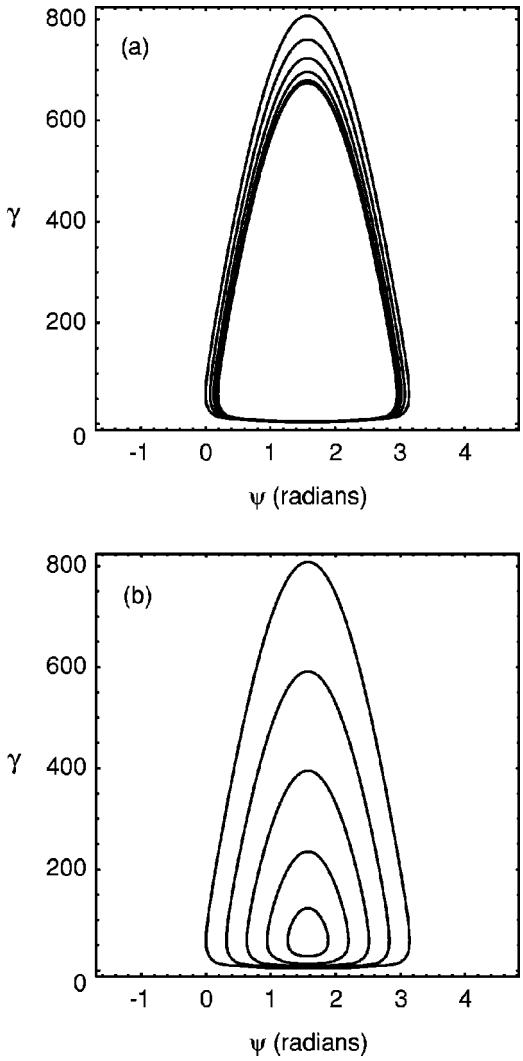

FIG. 4. Particle orbits in a wave with $e\phi_0/mc^2=0.1$ for (a) injection at 2.1 MeV and (b) injection at the group velocity corresponding to 30 MeV.

nonlinear evolution of the driving laser pulse. In one example the injected charge was set high enough to lead to substantial beamloading. The computational region is set in motion at the speed of light in order to approximately match the group velocity of the laser pulse.

A. Simulation of unphased injection

The simulation models a plasma channel with radial density profile $n(r)=n_0(1+r^2/r_{c1}^2)$, where $n_0=5\times10^{17}$ cm^{-3} and $r_{c1}=60$ μm. A step function is used for the axial density variation. The laser pulse has a radial amplitude variation $a(r)=a_0\exp(-r^2/r_0^2)$ with $r_0=30$ μm. This satisfies the matched beam condition $r_0=r_M$ where [4]

$$r_M=\left(\frac{r_{c1}^2}{\pi n_0 r_e}\right)^{1/4}, \tag{18}$$

with r_e the classical electron radius. The pulse duration is chosen to satisfy $\tau_L=\pi/\omega_p=80$ fs where τ_L is the full width half maximum (FWHM) pulse length, the pulse shape is the one described in Ref. [34], and ω_p is the on-axis plasma wavelength. The laser power is taken as $P_0=8$ TW. Several monoenergetic groups of electrons are introduced, each with a different initial kinetic energy $W_0=mc^2(\gamma_0-1)$. The characteristic transverse dimension of the electrons, r_{b0}, is chosen to coincide with the laser spot size r_0. The normalized emittance is taken as $\epsilon_{n0}=1\pi$ mm mrad. For the simulations discussed here and in the next section the injected charge was negligible.

Figure 5(a) shows contours of laser intensity at injection and the location of a group of unphased 1.6-MeV injected electrons at the entrance of the plasma channel ($z=0$) in the two-dimensional (slab) coordinate system. Here x is the axial coordinate in the moving window, y is the transverse coordinate, and the laser pulse moves to the right. The plasma wavelength $\lambda_p=2\pi c/\omega_p$ at this density is 47 μm, so the injected electron bunch covers more than one acceleration period, and particles are loaded over all phases. Figure 5(b) shows the laser pulse and particles when the front of the moving window is at $z'=ct=3.46$ cm. As a result of the matched injection into the plasma channel, the laser pulse is essentially unchanged. However, those electrons that have survived have been strongly focused and phase bunched into two short bunches that are confined to a region near the axis and are $\approx$30 times more dense than the original beam. The tendency of the wakefield to strongly bunch the particles helps minimize the energy spread by forcing all particles to experience nearly the same accelerating field.

Figure 6(a) plots the energy spectrum of the 1.6-MeV injected electrons at the same propagation distance ($z=3.46$ cm) and at the nominal dephasing length ($z=6.62$ cm). The spectrum at the first location has a narrow energy spread and an average energy of 225 MeV. At the second location, the average energy has approximately doubled to 406 MeV with an rms spread of 4.9%. Figure 6(b) shows a similar plot for an injection energy of 3.6 MeV. The higher injection energy results in a significantly broader energy spread and a reduction in the energy gain. For example, at $z=6.62$ cm, the mean energy is only 320 MeV and the relative energy spread $\Delta W/W_0=0.236$. The collection efficiency is significantly higher, however.

The simulation also gives the phasing between the focusing and accelerating phases of the wake. Figure 7(a) illustrates the phasing in a uniform plasma, and Fig. 7(b) illustrates the phasing in a plasma channel. Both panels are a false color image of the longitudinal field with a translucent gray overlay indicating the transverse fields. The red regions are accelerating, the blue regions are decelerating, and the grayed over regions are defocusing. In the uniform plasma, the intersection of the accelerating region with the (white) focusing region occupies approximately 90° of phase near the axis. In terms of the Hamiltonian model, this would correspond to taking $\psi_-=0$ and $\psi_+=\pi/2$. In the channel, by contrast, the focusing region not only occupies slightly more phase than the defocusing region, but is also shifted toward the accelerating region. In the particular case considered here, the focusing region lies between $\psi_-=-0.75$ and $\psi_+=2.65$, with focusing and acceleration occurring for -0.75

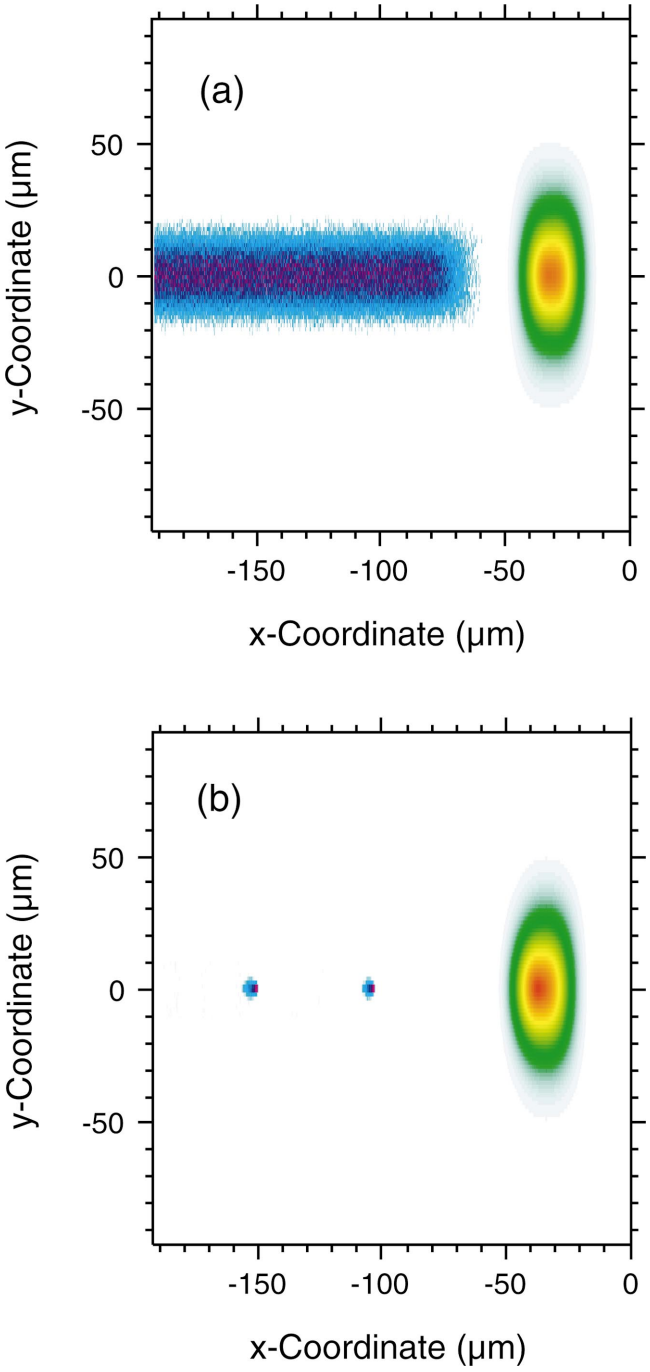

FIG. 5. (Color) Bunching of unphased monoenergetic electrons. Shown in (a) is a false color image of the laser intensity (red) and the electron density (purple) at the start of the simulation. Shown in (b) is the same image after 3.46 cm of propagation in the plasma channel. The highest electron density in (b) is 30 times higher than that in (a).

$<\psi<1.57$. In fact, the intersection of the focusing and accelerating regions is 48% larger than the same intersection in a uniform plasma.

It is interesting to note that using $\psi_-=-0.75$, $\psi_+=2.65$, and $W_0=1.6$ MeV in Eq. (10) gives $L_d=10.5$ cm. This is substantially longer than the classical dephasing length of 6.62 cm. The reason for the disparity is actually twofold.

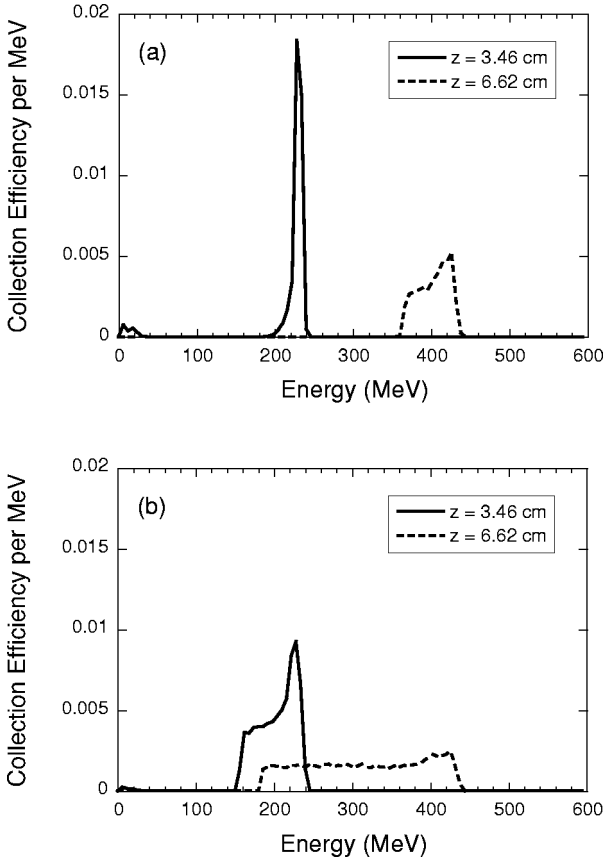

FIG. 6. Electron energy distributions after 3.46 cm of acceleration (solid line) and 6.62 cm of acceleration (dashed line) for (a) electrons injected at 1.6 MeV and (b) electrons injected at 3.6 MeV.

First, the classical dephasing length assumes $\psi_-=0$ and $\psi_+=\pi/2$. Second, the classical dephasing length assumes that the particle travels at the speed of light throughout the entire interaction. In both calculations, the finite spot size correction to the group velocity was accounted for.

B. Comparison of simulations with Hamiltonian model

The simulations discussed above confirmed the expectation that the laser pulse evolves very little during the interaction and that the injected electrons stay near the axis once they survive the initial bunching and pruning process. A quantitative comparison of the simulation results with the predictions of the quasi-2D Hamiltonian model is therefore appropriate. The simulation is as in the previous section, except this time the particles are loaded uniformly over exactly 2π radians of phase. For the Hamiltonian model, we take $\phi_0=0.1$, $\lambda_p/\lambda=59$, and the phase velocity of the wake is assumed to be at the spot-size-corrected group velocity of the laser pulse.

The solid line in Fig. 8 gives the collection efficiency η from the Hamiltonian model as a function of injection energy W_0, using Eqs. (3) and (4). The solid squares give the corresponding collection efficiences from the simulation. The agreement is excellent, particularly in terms of the ability to predict the minimum injection energy and the location of the

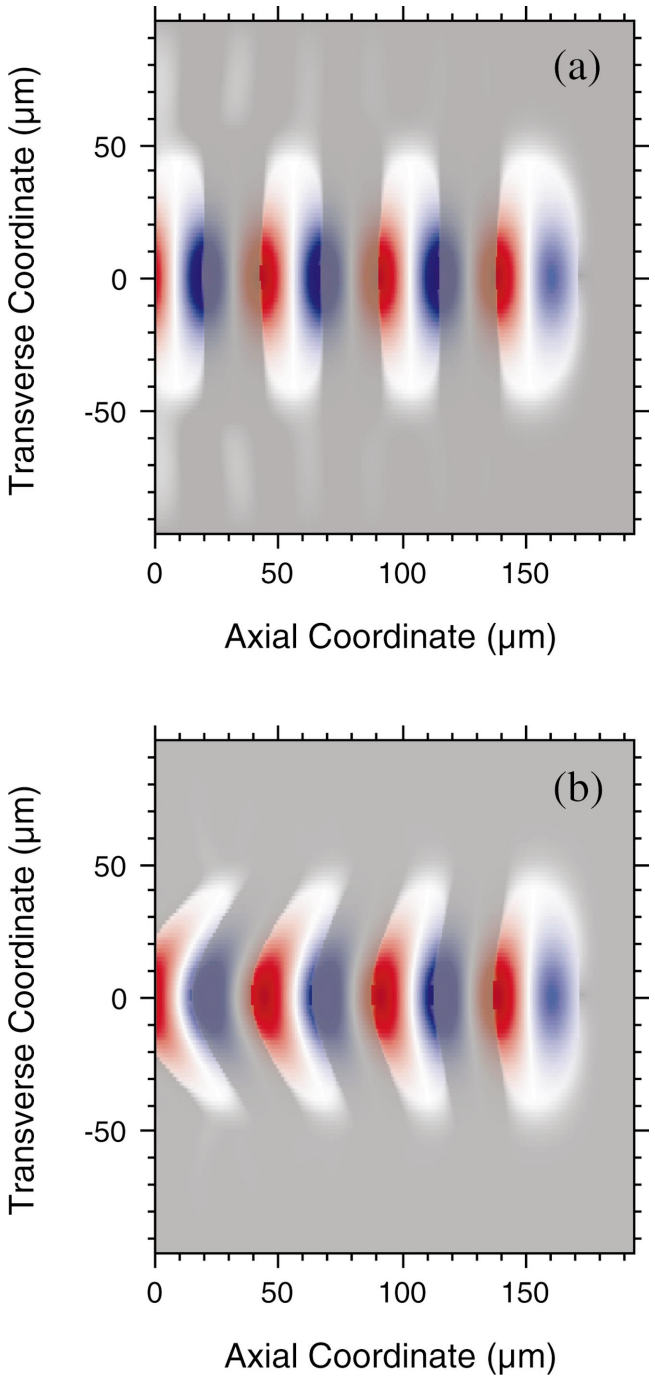

FIG. 7. (Color) Phase relationship between accelerating and focusing fields: (a) uniform plasma, (b) plasma channel.

"knee" in the curve. Furthermore, the quantitative errors are only about 10%. The dashed line in Fig. 8 gives the relative energy spread $\delta\gamma/\langle\gamma\rangle$ from Eqs. (13) and (14), and the open circles are from the simulation. For low injection energies, the quantitative errors are again about 10%, although at higher injection energies ($W_0=8$ MeV) the error rises to 40%.

Figure 9 compares the mean final energy $\langle W_f\rangle = mc^2(\langle\gamma_f\rangle - 1)$ and rms electron bunch length $\delta\psi_f$ as computed by TurboWAVE and the Hamiltonian model. The solid curve gives the mean final energy from Eq. (13), and the solid squares

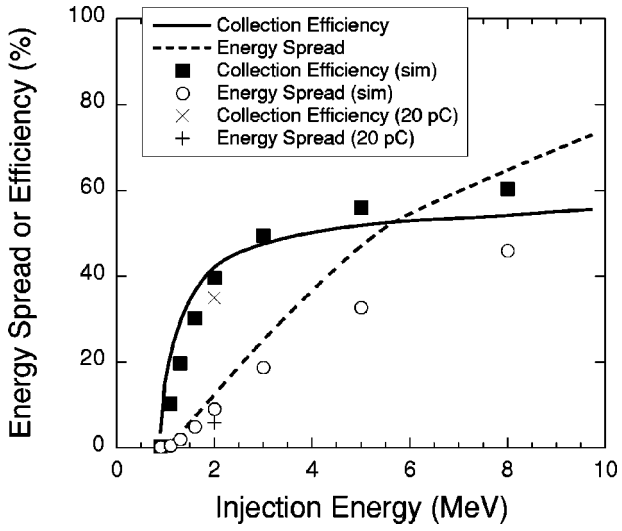

FIG. 8. Comparison of energy spread and collection efficiency vs injection energy as computed by the Hamiltonian model and the particle-in-cell simulation. The plus and the cross correspond to a case where beam-loading effects were included in the simulation.

are the simulation values. There is a significant drop in the final energy as the injection energy is increased. This reflects the collection of electrons over a broader range of phases, which results in some electrons actually being decelerated as the propagation distance approaches the classical dephasing length. The dashed curve plots the final rms normalized bunch length from Eq. (16), and the open circles are the simulation values. As expected, the bunch length is extremely short for injection energies just above the minimum injection energy. For example, when the injection energy is 1.6 MeV, the final phase spread is $\delta\psi_f=9.3°$, which corresponds to a bunch length of about 4 fs.

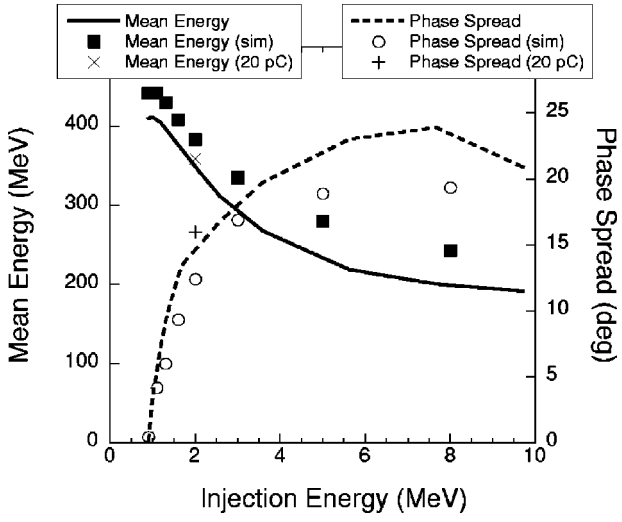

FIG. 9. Comparison of mean energy and bunch length vs injection energy as computed by the Hamiltonian model and the particle-in-cell simulation. The plus and the cross correspond to a case where beam-loading effects were included in the simulation.

C. Example with beam loading

To determine whether unphased monochromatic injection remains effective when beam loading is taken into account, we repeat the above simulation for 2 MeV injection with a peak electron beam density of $n_b = n_0/100 = 5 \times 10^{15}$ cm^{-3}. The total charge injected was 8.5 nC/cm, which in three dimensions would translate to about 20 pC. This corresponds to about 68% of the one-dimensional beam-loading limit [37]

$$N_0 = 5 \times 10^5 \left(\frac{n_1}{n_0} \right) \sqrt{n_0} A,$$

where N_0 is the number of electrons in the bunch, n_1 is the density perturbation due to the wake, n_0 is the ambient density, and A is the cross sectional area of the beam (units are cgs). The results from the simulation are shown in Figs. 8 and 9. The collection efficiency, mean energy, and phase spread are all affected unfavorably, but the change is not drastic. More interestingly, the energy spread is reduced significantly from the value obtained in the test particle limit. This can be understood by considering the fact that while the wake tends to accelerate particles at the back of the bunch more than at the front, the self-fields tend to accelerate particles at the front and decelerate those at the back. In other words, the self-fields tend to cancel out the nonuniformity of the wake. Since the nonuniformity of the wake is what causes the energy spread to grow, this partial cancellation helps keep the energy spread narrow. Based on this understanding, it appears likely that there is an optimum beam current which leads to a minimization of the energy spread. We leave this and other beam-loading issues for future study.

V. CONCLUSIONS

Channel guided laser wakefield accelerators can produce high-quality electron beams even in cases where the injected particles are uniformly loaded over all phases. By selecting the appropriate injection energy, a trade-off can be made between the charge collected and the final energy spread. The trade-off is very favorable in that as the injection energy is increased, the charge collected rises much more rapidly than the energy spread. This is a result not only of the strong phase bunching forces exerted by the wakefield, but also of a phase shift in the focusing fields induced by the presence of the channel. If the phasing of the focusing fields is known, a Hamiltonian formulation can be used to predict the mean energy, energy spread, mean phase, and phase spread of the accelerated electrons. The predictions of the Hamiltonian formulation agree well with 2D particle-in-cell simulations. Finally, the effects of beam loading can actually help to reduce the final energy spread on the beam.

The practical implication of this work is that a high-quality channel-guided LWFA might be built using relatively conventional technology as the source of externally injected electrons. Technologies such as dc- or rf-driven photocathodes might provide a suitable high-charge injection pulse more reliably than other more exotic schemes.

ACKNOWLEDGMENTS

Discussions with A. Zigler, T. G. Jones, D. Kaganovich, J. R. Peñano, R. Tempkin, J. Rosenzweig, and A. G. Khachatryan are gratefully acknowledged. This work was supported by the Division of High Energy Physics, Office of Energy Research, U.S. Department of Energy, the Office of Naval Research, and a DOE Small Business Innovation Research (SBIR) Grant to Icarus Research, Inc..

[1] T. Tajima and J. M. Dawson, Phys. Rev. Lett. **43**, 267 (1979).
[2] P. Sprangle, E. Esarey, A. Ting, and G. Joyce, Appl. Phys. Lett. **53**, 2146 (1988).
[3] E. Esarey, P. Sprangle, J. Krall, and A. Ting, IEEE Trans. Plasma Sci. **24**, 252 (1996).
[4] H. Milchberg, T. Clark, C. Durfee, T. Antonsen, and P. Mora, Phys. Plasmas **3**, 2149 (1996).
[5] Y. Ehrlich, C. Cohen, A. Zigler, J. Krall, P. Sprangle, and E. Esarey, Phys. Rev. Lett. **77**, 4186 (1996).
[6] D. Kaganovich, A. Ting, C. Moore, A. Zigler, H. Burris, Y. Ehrlich, R. Hubbard, and P. Sprangle, Phys. Rev. E **59**, R4769 (1999).
[7] E. Gaul, S. L. Blanc, A. Rundquist, R. Zgadzaj, H. Langhoff, and M. Downer, Appl. Phys. Lett. **77**, 4112 (2000).
[8] P. Volfbeyn, E. Esarey, and W. Leemans, Phys. Plasmas **6**, 2269 (1999).
[9] Y. Kitagawa *et al.*, Phys. Rev. Lett. **92**, 205002 (2004).
[10] D. Strickland and G. Mourou, Opt. Commun. **56**, 219 (1985).
[11] D. Umstadter, Phys. Plasmas **8**, 1774 (2001).
[12] W. Leemans, P. Volfbeyn, K. Guo, S. Chattopadhyay, C. Shroeder, B. Shadwick, P. Lee, J. Wurtele, and E. Esarey, Phys. Plasmas **5**, 1615 (1998).
[13] R. Hubbard, P. Sprangle, and B. Hafizi, IEEE Trans. Plasma Sci. **28**, 1122 (2000).
[14] R. Hubbard, D. Kaganovich, B. Hafizi, C. Moore, P. Sprangle, A. Ting, and A. Zigler, Phys. Rev. E **63**, 036502 (2001).
[15] P. Sprangle, J. Peñano, B. Hafizi, R. Hubbard, A. Ting, D. Gordon, A. Zigler, and T. Antonsen, Phys. Plasmas **9**, 2364 (2002).
[16] A. Modena *et al.*, IEEE Trans. Plasma Sci. **24**, 289 (1996).
[17] C. I. Moore, A. Ting, K. Krushelnick, E. Esarey, R. F. Hubbard, B. Hafizi, H. R. Burris, C. Manka, and P. Sprangle, Phys. Rev. Lett. **79**, 3909 (1997).
[18] S.-Y. Chen, G. Sarkisov, A. Maksimchuk, R. Wagner, and D. Umstadter, Phys. Rev. Lett. **80**, 2610 (1998).
[19] D. Gordon *et al.*, Phys. Rev. Lett. **80**, 2133 (1998).
[20] A. Pukhov and J. Meyer-ter-Vehn, Appl. Phys. B: Lasers Opt. **74**, 355 (2002).
[21] A. Zhidkov, J. Koga, K. Kinoshita, and M. Uesaka, Phys. Rev. E **69**, 035401 (2004).
[22] S. Mangles *et al.*, Nature (London) **431**, 535 (2004).
[23] C. Geddes, C. Toth, J. van Tilborg, E. Esarey, C. Schroeder, D. Bruhwiler, C. Nieter, J. Cary, and W. Leemans, Nature (London) **431**, 538 (2004).

[24] J. Faure, Y. Glinec, A. Pukhov, S. Kiselev, S. Gordienko, E. Lefebvre, J. Rousseau, F. Burgy, and V. Malka, Nature (London) **431**, 541 (2004).
[25] P. Sprangle, B. Hafizi, J. Peñano, R. Hubbard, A. Ting, C. Moore, D. Gordon, A. Zigler, D. Kaganovich, and T. Antonsen, Jr., Phys. Rev. E **63**, 056405 (2002).
[26] A. Khachatryan, Phys. Rev. E **65**, 046504 (2002).
[27] A. Reitsma, W. Leemans, E. Esarey, C. Schroeder, L. Kamp, and T. Schep, Phys. Rev. ST Accel. Beams **5**, 051301 (2002).
[28] R. F. Hubbard, D. F. Gordon, T. G. Jones, J. R. Peñano, P. Sprangle, A. Ting, B. Hafizi, A. Zigler, and D. Kaganovich (unpublished).
[29] D. Umstadter, J. K. Kim, and E. Dodd, Phys. Rev. Lett. **76**, 2073 (1996).
[30] E. Esarey, R. F. Hubbard, W. P. Leemans, A. Ting, and P. Sprangle, Phys. Rev. Lett. **79**, 2682 (1997).
[31] C. I. Moore, A. Ting, T. Jones, E. Briscoe, B. Hafizi, R. F. Hubbard, and P. Sprangle, Phys. Plasmas **8**, 2481 (2001).
[32] D. F. Gordon, A. Ting, T. Jones, B. Hafizi, R. Hubbard, and P. Sprangle (unpublished).
[33] S. Eisenmann *et al.* (unpublished).
[34] D. F. Gordon, W. B. Mori, and T. M. Antonsen, Jr., IEEE Trans. Plasma Sci. **28**, 1224 (2000).
[35] N. E. Andreev, L. M. Gorbunov, V. I. Kirsanov, K. Nakajima, and A. Ogata, Phys. Plasmas **4**, 1145 (1997).
[36] E. Esarey and M. Pilloff, Phys. Plasmas **2**, 1432 (1995).
[37] T. Katsouleas, S. Wilks, P. Chen, J. Dawson, and J. Su, Part. Accel. **22**, 81 (1987).